

Super-resolved imaging with ultimate time resolution

Yuto Ashida¹ and Masahito Ueda^{1,2}

¹*Department of Physics, University of Tokyo,
7-3-1 Hongo, Bunkyo-ku, Tokyo 113-0033, Japan*

²*Center for Emergent Matter Science (CEMS),
RIKEN, Wako, Saitama 351-0198, Japan*

Abstract

Precisely and accurately locating point objects is a long-standing common thread in science. Super-resolved imaging of single molecules [1–3] has revolutionized our view of quasi-static nanostructures *in-vivo*. A wide-field approach based on localizing individual fluorophores has emerged as a versatile method [4–8] to surpass the standard resolution limit [9, 10]. In those techniques, the super-resolution is realized by sparse photoactivation and localization together with the statistical analysis based on point spread functions. Nevertheless, the slow temporal resolution of super-resolved imaging severely restricts the utility to the study of live-cell phenomena. Clearly, a major breakthrough to observe fast, nanoscale dynamics needs to be made. Here we present a super-resolved imaging method that achieves the theoretical-limit time resolution. By invoking information theory, we can achieve the robust localization of overlapped light emitters at an order of magnitude faster speed than the conventional super-resolution microscopy. Our method thus provides a general way to uncover hidden structures below the diffraction limit and should have a wide range of applications in all disciplines of science and technology [11–15].

I. INTORDUCTION

Ever since the discovery of the diffraction limit [9], the attempts of surpassing the diffraction barrier have long occupied a major part of research in wide areas of life science, physics, chemistry, and astronomy. Recent experimental achievements of super-resolved imaging have stimulated theoretical research to challenge this limit. The ultimate resolution to the problem, i.e., the accurate localization of multiple point objects regardless of the degree of overlap, should allow the super-resolved imaging at the theoretical-limit time resolution and significantly advance the research of dynamical subcellular phenomena. Examples include the study of protein interactions in the mitochondria and real-time observation of gene expression regulation inside the nucleus [16].

The single-molecule localization microscopy (SMLM) works under conditions in which fluorescent molecules are activated at very low density so that no more than a single molecule within any diffraction-limited region emits photons simultaneously [17, 18]. A set of single-molecule positions can then be precisely determined beyond the diffraction limit by fitting each image of molecules using a single point spread function. This analysis discards the information from crowded molecules with overlapping images through filtering. Typically, SMLM requires accumulating thousands of frames to generate a super-resolution image, resulting in the long image acquisition time [16, 19, 20].

Molecular interactions occur on nanoscale, and every life phenomenon can, in principle, be characterized by the set of coordinates of individual biomolecules. Hence, to achieve a real-time observation of intracellular molecule dynamics at this scale has long been a holy grail in life science. If the dynamics of the structure is not of interest, drift motion during the long imaging time of SMLM causes artifacts [21] and a substantial reduction of the imaging time will significantly expand the horizon of super-resolution techniques. To achieve these goals, a major breakthrough based on principles different from SMLM is needed.

II. RESULTS

We develop a super-resolved imaging method that achieves simultaneous localization of substantially overlapping light emitters at the theoretical-limit speed. In a previous work, we show that tracking progressive collapse of many-body wavefunction enables a

diffraction-unlimited position measurement of ultracold atoms [12] in an optical lattice. We here drastically generalize this approach to classical objects, such as fluorescent molecules, by treating the estimated position distribution as a counterpart of the quantum-mechanical wavefunction. To demonstrate how superior our simultaneous localization approach is to the conventional SMLM, we show a typical result in Fig. 1. While SMLM can only identify the well-isolated molecules as indicated by the circles in Fig. 1a, our method identifies all molecules at the theoretical-limit precision as shown in Fig. 1b. Hence, our approach allows an accurate and precise localization of multi-emitters despite a substantial overlap of images. Our method thus enables us to increase the image molecule density at each frame, which in turn reduces the acquisition time by an order of magnitude, achieving the theoretical-limit time resolution as discussed below.

While there have recently been remarkable progresses in improving temporal resolution [22–25], they suffer low fidelity and low spatial resolution due to difficulties of accurate and precise simultaneous localization of multi-emitters. In contrast, our method efficiently achieves the theoretical limit of precision even at high image molecule density and, hence, provides a unique way for the ultimate-time-resolved super-resolution microscopy. To clarify this point, let us discuss the theoretical limit on temporal resolution of super-resolved imaging. The image acquisition time of super-resolution microscopy is determined by two key

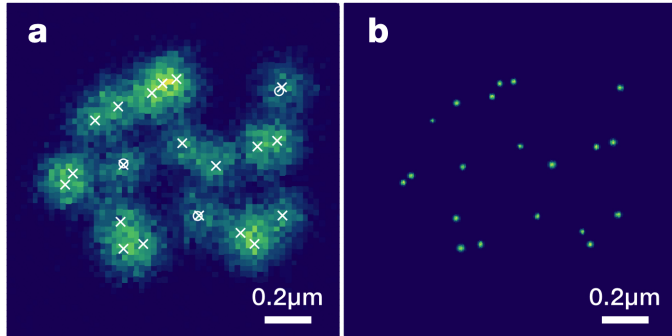


FIG. 1. Demonstration of simultaneous localization of overlapping light emitters. **a**, A single simulated image of fluorescent molecules with uniform background noise. The crosses indicate the true positions of particles. The conventional technique (SMLM) can only identify well-isolated emitters as indicated by circles. **b**, The result of our simultaneous localization. Despite a substantial overlap of the interference patterns as shown in Fig. 1a, our method identifies all molecules at the theoretical-limit precision.

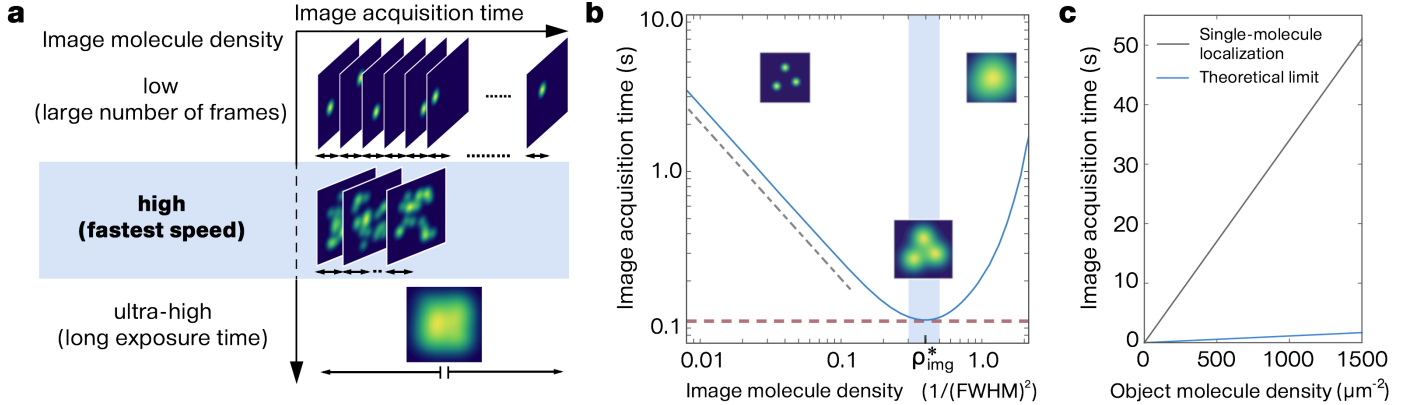


FIG. 2. **Theoretical limit on the time resolution of super-resolution microscopy.**

a, High image molecule density allows the fastest image acquisition. Single-molecule localization microscopy, which works at low image molecule density, requires a large number of frames, resulting in a low temporal resolution. Ultra-high image density requires a huge number of photodetections due to drastic reduction in information gain per photon, resulting in a long exposure time. **b**, Theoretical limit on the image acquisition time. In a low-density region, increasing an image density reduces the image acquisition time according to the scaling $\propto \rho_{\text{img}}^{-1}$. In an ultra-high density region, the required number of signals dramatically increases as the interference pattern begins to overlap, leading to a rapid increase in the image acquisition time. The fastest imaging can be achieved inbetween, which sets the theoretical limit indicated by the red-dashed line. The desired precision δ is 10 nm and the object molecule density ρ_{obj} is $100 \mu\text{m}^{-2}$. **c**, Super-resolved imaging with ultimate time resolution. A high image molecule density enables an order of magnitude faster imaging than the conventional (SMLM) technique.

quantities: the number of frames to generate a super-resolution image [26] and the exposure time for a single frame of independently activated molecules. The former is determined by the ratio between the object molecule density ρ_{obj} and the image molecule density ρ_{img} at each frame. The latter is equal to the collection time of photons required to achieve the desired spatial resolution. The minimum number of photons is given by the ratio between the desired precision and the amount of information provided by a single photodetection (Methods section).

Figure 2a summarizes the theoretical limit on the time resolution of super-resolution microscopy for varying image density. In a low-density region, where the activated molecules

are sparsely distributed so that the interference patterns rarely overlap, the amount of information carried by a single photon is nearly constant. Thus, increasing an image density directly reduces the acquisition time for a super-resolution image which scales as $\propto \rho_{\text{img}}^{-1}$. However, as the interference patterns begin to overlap, the information gain per photon dwindles rapidly. Consequently, the required number of photons rapidly increases, resulting in a sharp increase in the image acquisition time. Hence, the fastest time resolution is achieved at a high image density between the above two situations, where the information acquisition rate is maximal. The crucial point is that our simultaneous localization analysis can achieve both high fidelity and the fundamental precision limit at this density region as detailed later.

We now describe our method in more detail. The effective point spread function (PSF) of a single molecule is a two-dimensional Gaussian with a full-width at half-maximum [27] (FWHM) of $\sigma_{\text{HM}} = 2.35 \times 0.21\lambda/\text{NA}$ ($=194\text{nm}$ for a wavelength of the probe light $\lambda = 550\text{nm}$ and a numerical aperture of a lens $\text{NA}=1.4$). The interference pattern of multi-emitters is constructed from an incoherent sum of these point spread functions. We consider imaging as a stochastic process where spatial locations of photodetections are stochastically generated according to the interference pattern. Although we assume, for simplicity, that emitters are equally bright and the background noise is uniform, the following discussions can easily be modified to more general cases (see Appendices).

The theoretical limit on the image acquisition time to achieve the spatial precision δ is given by (Methods section),

$$T_{\text{img}} \geq T_{\min}(\rho_{\text{obj}}, \sigma_{\text{HM}}, \delta). \quad (1)$$

The ultimate limit T_{\min} is obtained by the minimum of the information-theoretical lower bound of the image acquisition time (Fig. 2b). The optimal image density ρ_{img}^* depends on the diffraction limit of an optical system σ_{HM} and is independent of any other details such as the density of object molecules and the desired spatial precision. Figure 2c compares the achievable theoretical limit of the time resolution with that of the conventional SMLM for typical experimental parameters. Ultimately, super-resolved imaging can be performed by a factor of thirty faster than the conventional techniques [3–5]. To extract the maximum information about the positions of multi-emitters regardless of the degree of overlap, we also need a reliable criteria to determine the number of molecules in the area of our interest in

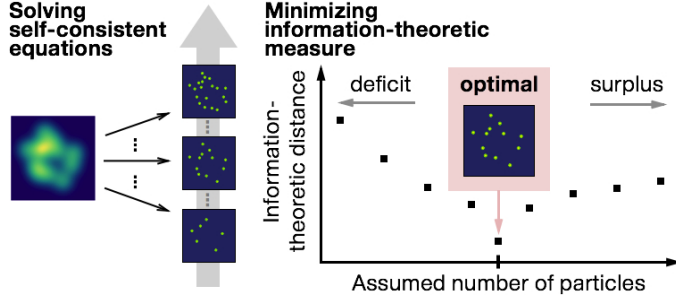


FIG. 3. **Unbiased, simultaneous localization of multi-emitters.** The set of the positions of particles compatible with the observed data is determined by solving the self-consistent equations for the varying total number of particles. The final estimated positions are determined by minimizing the Kullback-Leibler divergence between the observed data and the expected interference pattern for the candidate set of positions. This automatically gives the optimal particle number because any misidentification implies deficit or surplus of particles, which increases the information-theoretic distance.

addition to the precise localization of each emitter's coordinate.

III. SIMULTANEOUS LOCALIZATION AND SIMULATION

The unbiased simultaneous localization of multi-emitters at the fundamental precision limit can be achieved by invoking information theory. Figure 3 summarizes the principle of the analysis. A complete set of the numbers of photodetections at individual pixels constitute the sufficient statistic and the problem reduces to solving the self-consistent equations for the molecule positions. First, for the varying number of point sources, a set of positions are generated by solving the self-consistent equations with a fast high-order iterative method. The solutions can be shown to coincide with the maximum likelihood estimators generated by the same observed data (see Appendix). Second, the probability distribution of photodetections for each set of positions is calculated, and compared with the observed distribution. This is done based on the information-theoretic measure called the Kullback-Leibler divergence. The total particle number is then determined by minimizing this measure because an insufficient or a surplus number of estimators results in a distribution different from the actual interference pattern. In this way, the global spatial information of the acquired pattern is automatically taken into account to accurately determine the total molecule number. The

analysis can also be extended to three-dimensional astigmatic imaging [28] (see Appendix for details).

To achieve the fundamental limit of time resolution in Eq. (1), the crucial fact is that our simultaneous localization significantly outperforms the single-molecule analysis at high density region, where super-resolved imaging can be performed with ultimate time resolution. The simultaneous localization analysis attains more than a tenfold improvement of the fraction of identified molecules with respect to the conventional single-molecule analysis (Fig. 4a). The simulation result is the average taken over randomly generated different

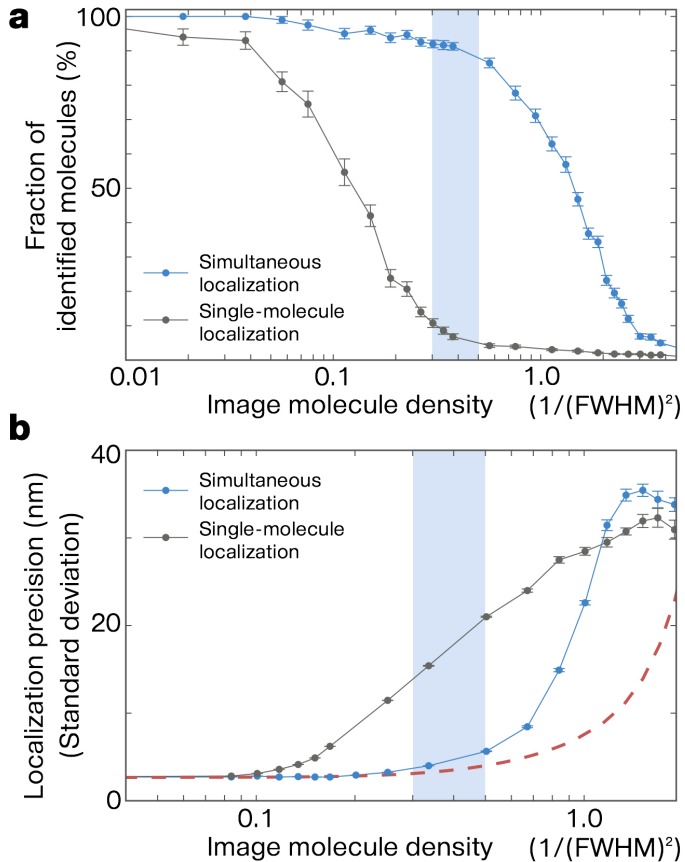


FIG. 4. **Performance of the simultaneous localization.** **a**, The fraction of identified molecules and **b**, the localization precision are plotted against a normalized image molecule density. The result is compared with the conventional single-molecule localization. In **b**, the theoretical lower bound is shown by the red-dashed curve. The simultaneous localization significantly outperforms the single-molecule analysis at a high density region indicated by the blue-shaded area where the super-resolved imaging is performed with an ultimate time resolution.

configurations of molecules. In particular, some ninety percent accuracy is achieved in the region enabling the fastest super-resolved imaging. The simultaneous localization also achieves, in the region of the ultimate time resolution, the theoretical-limit precision (Fig. 4b). Note that, in the single-molecule analysis, only those emitters that are not rejected by the algorithm are taken into account in evaluating the localization precision; thus, a relatively high precision of SMLM at high density region is superficial. In contrast, in our simultaneous localization, the average is taken over all estimators. At an ultra-high density region where the density becomes larger than the optimal region and the images completely overlap, both analyses fail to identify and localize molecule positions. This is because the information gain carried by a photon almost vanishes and an extremely high signal-to-noise ratio is required to achieve the desired precision.

These results establish the fact that our analysis can accurately and precisely localize molecule positions at the theoretical limit. In principle, the fraction of identified molecules and the localization precision can be improved up to the fundamental limits by performing iterative calculations for sufficiently large number of different initial estimators (see Appendices).

IV. DISCUSSIONS

We have demonstrated that the information-theoretic analysis enables the super-resolved imaging with ultimate time resolution. The analysis successfully identifies the complete set of the positions of highly dense molecules despite a substantial overlap of interference patterns. Our information-theoretic treatment sets the fundamental limit on both spatial and temporal resolutions. In this way, our method achieves high spatial precision at the fundamental limit and an order of magnitude faster super-resolved imaging than the conventional techniques. The ultimate-time-resolved super-resolution microscopy will open up many possibilities such as real-time observation of intracellular phenomena at molecular scale. Finally, our method should also provide a powerful means to unveil detailed structures at the scale below the diffraction limit in all disciplines of science and technology [11–15].

V. METHODS

Theoretical limit on the time resolution of super-resolution microscopy. The image acquisition time T_{img} of localization-based super-resolution microscopy is determined by a number of frames and an exposure time of each frame. We define the fidelity F of super-resolved imaging as the fraction of imaged molecules i.e., activated molecules at least once during the imaging. Then the required number of frames to ensure the fidelity is given by $-\ln(1 - F)\rho_{\text{obj}}/\rho_{\text{img}}$, where ρ_{obj} (ρ_{img}) is the object (image) molecule density. An exposure time of a single frame is determined by the required number of photons $N_{\text{photon}}(\rho_{\text{img}}, \delta, \sigma)$ to achieve the desired resolution δ divided by the collection rate $\rho_{\text{img}}S\Gamma$, where S is the area of the region of interest and Γ is the collection rate of photons per molecule. Information theory dictates that N_{photon} be bounded by the Fisher information matrix. To obtain the net information gain, we calculate the diagonal element of the inverse of the Fisher information matrix $[\mathcal{I}^{-1}]_{DD}$ by assuming the arrayed configuration with density ρ_{img} . Then N_{photon} is bounded as

$$N_{\text{photon}}(\rho_{\text{img}}, \delta, \sigma) \geq \frac{1}{\delta^2}[\mathcal{I}^{-1}]_{DD} \equiv \frac{1}{\delta^2}\rho_{\text{img}}S\Delta^2(\rho_{\text{img}}, \sigma),$$

where we define the normalized precision limit Δ^2 by the last equality. For example, if molecules are sufficiently sparse, Δ^2 is equal to σ^2 , which is consistent with the single-molecule analysis. The information-theoretic limit on the image acquisition time is now obtained by

$$T_{\text{img}} \geq \ln\left(\frac{1}{1 - F}\right) \frac{\rho_{\text{obj}}}{\rho_{\text{img}}^*} \frac{\Delta^2(\rho_{\text{img}}^*, \sigma)}{\delta^2\Gamma},$$

where ρ_{img}^* is the optimized image density so that the lower-bound of the image acquisition time is minimized. The result is plotted for the required precision $\delta = 10\text{nm}$, fidelity $F = 0.9$, collection rate $\Gamma = 2.3 \times 10^4 \text{ 1/s}$, and the standard deviation of the point spread function $\sigma = 82.5\text{nm}$.

Simultaneous localization. We first solve, for the varying estimated molecule number N_{est} , the following self-consistent equations of estimated molecule positions $\mathbf{R}_1, \mathbf{R}_2, \dots, \mathbf{R}_{N_{\text{est}}}$:

$$\mathbf{R}_m = \frac{\sum_{\langle i,j \rangle} \mathbf{r}_{ij} g_{ij;m}(\mathbf{R}_1, \mathbf{R}_2, \dots, \mathbf{R}_{N_{\text{est}}})}{\sum_{\langle i,j \rangle} g_{ij;m}(\mathbf{R}_1, \mathbf{R}_2, \dots, \mathbf{R}_{N_{\text{est}}})},$$

where $\langle i, j \rangle$ is the label of pixels, \mathbf{r}_{ij} is the pixel position, $m = 1, 2, \dots, N_{\text{est}}$ labels each estimator, and we introduce the weight function $g_{ij;m}$ by

$$g_{ij;m} \equiv \frac{N_{ij} \exp\left(-\frac{|\mathbf{r}_{ij} - \mathbf{R}_m|^2}{2\sigma^2}\right)}{\gamma + \sum_{k=1}^{N_{\text{est}}} \exp\left(-\frac{|\mathbf{r}_{ij} - \mathbf{R}_k|^2}{2\sigma^2}\right)}.$$

Here we denote N_{ij} as the observed number of photodetections at the pixel $\langle i, j \rangle$, which constitutes the sufficient statistic, and introduce the term γ , which takes into account the contribution from the uniform background noise (see Appendix for details of the formulation). The solution is obtained by the higher-order iterative method, which allows fast convergence, and is shown to coincide with the maximum likelihood estimator. To make a robust convergence to the true solution, we repeatedly perform iterations from many different initial positions, which are generated through the following two stages.

First, well-separated molecules are pre-estimated and localized by the prior analysis, which finds a local maximum with a suitable threshold. These localized positions are taken as the first part of initial positions. Second, the residual part of initial positions, which corresponds to the difference between the assumed particle number and the pre-estimated emitter number at the first stage, are randomly generated according to the observed probability distribution of photodetections. A large number of different sets of initial positions are prepared and iterations are performed for each set. From these candidates of solutions, the correct solution is robustly selected by using the rejection algorithm based on the information-theoretic distance (see Appendices for details of methods).

We finally optimize the total particle number and identify a true set of emitter positions. This is done by minimizing the Kullback-Leibler divergence with respect to N_{est} :

$$\min_{N_{\text{est}}} D[P_{\text{data}} \parallel P_{N_{\text{est}}}],$$

where P_{data} is the normalized distribution of observed photodetections and $P_{N_{\text{est}}}$ is the reconstructed interference pattern with the solution of the equations for the number of molecules N_{est} .

The numerical simulations are performed for a simulated data of photodetections generated according to the interference pattern with a uniform background noise. The fraction of identified molecules and the localization precision are plotted against the image molecule density. The average is taken over 10000 stochastically generated different configurations of

particles. The simulation is performed for 1000 collected photons per molecule, 50 signal-to-noise ratio, and the standard deviation of the point spread function $\sigma = 82.5\text{nm}$. Details on the analyses can be also found in Appendices.

Acknowledgements

We are grateful for discussions with K. Goda, H. Mikami and T. Shitara. This work was supported by KAKENHI Grant No. 26287088 from the Japan Society for the Promotion of Science, and a Grant-in-Aid for Scientific Research on Innovation Areas “Topological Quantum Phenomena” (KAKENHI Grant No. 22103005), the Photon Frontier Network Program from MEXT of Japan, and the Mitsubishi Foundation.

- [1] Klar, T. A. *et al.* Fluorescence microscopy with diffraction resolution barrier broken by stimulated emission. *Proc. Natl Acad. Sci. USA* **97**, 8206–8210 (2000).
- [2] Gustafsson, M. G. L. Nonlinear structured-illumination microscopy: wide-field fluorescence imaging with theoretically unlimited resolution. *Proc. Natl Acad. Sci. USA* **102**, 13081–13086 (2005).
- [3] Betzig, E. *et al.* Imaging intracellular fluorescent proteins at nanometer resolution. *Science* **313**, 1642–1645 (2006).
- [4] Hess, S. T., Girirajan, T. P. K. & Mason, M. D. Ultra-high resolution imaging by fluorescence photoactivation localization microscopy. *Biophys. J.* **91**, 4258–4272 (2006).
- [5] Rust, M. J., Bates, M. & Zhuang, X. Sub-diffraction-limit imaging by stochastic optical reconstruction microscopy (STORM). *Nat. Met.* **10**, 793–795 (2006).
- [6] Bates, M., Huang, B., Dempsey, G. T. & Zhuang, X. Multicolor super-resolution imaging with photo-switchable fluorescent probes. *Science* **317**, 1749–1753 (2007).
- [7] Shroff, H. *et al.* Dual-color superresolution imaging of genetically expressed probes within individual adhesion complexes. *Proc. Natl Acad. Sci. USA* **104**, 20308–20313 (2007).
- [8] Pertsinidis, A., Zhang, Y. & Chu, S. Subnanometre single-molecule localization, registration and distance measurements. *Nature* **466**, 647–651 (2010).
- [9] Abbe, E. Beitrage zur Theorie des Mikroskops und der mikroskopischen Wahrnehmung. *Arch. Mikroskop. Anat.* **9**, 413 (1873).

[10] Born, M. *et al.* *Principles of Optics: Electromagnetic Theory of Propagation, Interference and Diffraction of Light* (Cambridge Univ. Press, 1999).

[11] Bakr, W. S. *et al.* A quantum gas microscope for detecting single atoms in a Hubbard-regime optical lattice. *Nature* **462**, 74–77 (2009).

[12] Ashida, Y. & Ueda, M. Diffraction-unlimited position measurement of quantum particles. Preprint at <http://arxiv.org/abs/1409.8399> (2014).

[13] Richardson, W. H. Bayesian-based iterative method of image restoration. *J. Opt. Soc. Amer.* **62**, 55–59 (1972).

[14] Lucy, L. B. An iterative technique for the rectification of observed distributions. *Astron. J.* **79**, 745–754 (1974).

[15] Billinge, S. J. L. & Levin, I. The problem with determining atomic structure at the nanoscale. *Science* **316**, 561–565 (2007).

[16] Huang, B., Babcock, H. & Zhuang, X. Breaking the diffraction barrier: super-resolution imaging of cells. *Cell* **143**, 1047–1058 (2010).

[17] Betzig, E. Proposed method for molecular optical imaging. *Opt. Lett.* **20**, 237–239 (1995).

[18] Patterson, G., Davidson, M., Manley, S. & Lippincott-Schwartz, J. Superresolution imaging using single-molecule localization. *Annu. Rev. Phys. Chem.* **61**, 345–367 (2010).

[19] Moerner, W. E. Eyes on super-resolution. *Nat. Photon.* **3**, 368–369 (2009).

[20] Schermelleh, L., Heintzmann, R. & Leonhardt, H. A guide to super-resolution fluorescence microscopy. *J. Cell Bio.* **190**, 165–175 (2010).

[21] Deschout, H. *et al.* Precisely and accurately localizing single emitters in fluorescence microscopy. *Nat. Met.* **11**, 253–266 (2014).

[22] Holden, S. J., Uphoff, S. & Kapanidis, A. N. DAOSTORM: an algorithm for high-density super-resolution microscopy. *Nat. Met.* **8**, 279–280 (2011).

[23] Quan, T. *et al.* High-density localization of active molecules using structured sparse model and Bayesian information criterion. *Opt. Exp.* **19**, 16963–16974 (2011).

[24] Cox, S. *et al.* Bayesian localization microscopy reveals nanoscale podosome dynamics. *Nat. Met.* **9**, 195–200 (2012).

[25] Huang, F. *et al.* Video-rate nanoscopy using sCMOS camera-specific single-molecule localization algorithms. *Nat. Met.* **10**, 653–658 (2013).

[26] Small, A. R. Theoretical limits on errors and acquisition rates in localizing switchable fluo-

rophores. *Biophys. J.* **96**, L16–L18 (2009).

[27] Zhang, B., Zerubia, J. & Olivo-Marin, J.-C. Gaussian approximations of fluorescence microscope point-spread function models. *Appl. Opt.* **46**, 1819–1829 (2007).

[28] Holtzer, L., Meckel, T. & Schimidt, T. Nanometric three-dimensional tracking of individual quantum dots in cells. *Appl. Phys. Lett.* **90**, 053902 (2007).

Appendix A: Formulation of the model

Here we formulate the imaging as a stochastic process in which spatial locations of photodetections are randomly generated according to the interference pattern. The effective point spread function of a single molecule is described by two-dimensional Gaussian function:

$$P[\mathbf{r}|\mathbf{R}] = \frac{1}{2\pi\sigma^2} \exp\left(-\frac{|\mathbf{r} - \mathbf{R}|^2}{2\sigma^2}\right), \quad (\text{A1})$$

where $\sigma = 0.21\lambda/\text{NA}$ is the standard deviation of the point spread function with NA being the numerical aperture, and we denote the position of the molecule as $\mathbf{R} = (X, Y)^T$ and that of photodetections as $\mathbf{r} = (x, y)^T$. We first assume that molecules are equally bright and the background noise is uniformly distributed; we shall discuss a more general case later. The discussions will be also extended to three-dimensional imaging.

The probability distribution of photodetections $P[\mathbf{r}|\{\mathbf{R}\}]$ generated by multiple N molecules positioned at $\{\mathbf{R}\} \equiv \{\mathbf{R}_1, \mathbf{R}_2, \dots, \mathbf{R}_N\}$ is constructed from an incoherent sum of the individual point-spread functions:

$$P[\mathbf{r}|\{\mathbf{R}\}] = \frac{1 - \epsilon}{N} \sum_{m=1}^N P[\mathbf{r}|\mathbf{R}_m] + \frac{\epsilon}{S}. \quad (\text{A2})$$

Here ϵ is the fraction of the background noise, which can be related to the signal-to-noise ratio (SNR) as $\epsilon = 1/(1 + \text{SNR})$, and S is the area of the region of interest.

Let us assume that N_{photon} photons are detected at $\mathbf{r}_1, \mathbf{r}_2, \dots, \mathbf{r}_{N_{\text{photon}}}$ with probability distribution $P[\mathbf{r}_1, \mathbf{r}_2, \dots, \mathbf{r}_{N_{\text{photon}}}]$. The conditional probability distribution of a set of N_{est} molecule estimators $\{\mathbf{R}\}_{\text{est}}$ is given by the Bayesian inference:

$$P[\{\mathbf{R}\}_{\text{est}}|\mathbf{r}_1, \mathbf{r}_2, \dots, \mathbf{r}_{N_{\text{photon}}}] = \frac{\prod_{i=1}^{N_{\text{photon}}} P[\mathbf{r}_i|\{\mathbf{R}\}_{\text{est}}] P_0[\{\mathbf{R}\}_{\text{est}}]}{P[\mathbf{r}_1, \mathbf{r}_2, \dots, \mathbf{r}_{N_{\text{photon}}}]}, \quad (\text{A3})$$

where $P_0[\{\mathbf{R}\}_{\text{est}}]$ represents a prior distribution of the molecule distribution.

Appendix B: Fisher information matrix and Cramér-Rao bound

Information theory tells us that the variance-covariance matrix of any unbiased estimators is bounded by the acquired information quantity:

$$\text{Cov}_{\boldsymbol{\theta}}[\hat{\boldsymbol{\theta}}] \geq \frac{\mathcal{I}^{-1}[\boldsymbol{\theta}]}{n}. \quad (\text{B1})$$

$\text{Cov}_{\boldsymbol{\theta}}[\hat{\boldsymbol{\theta}}]$ denotes the variance-covariance matrix of estimators $\hat{\boldsymbol{\theta}}$, \mathcal{I}^{-1} is the inverse matrix of the Fisher information matrix, and n is the number of data points. The matrix inequality is to be understood to mean that the matrix obtained by subtracting the right-hand side from the left-hand side is positive semidefinite. The right-hand side sets the information-theoretical limit of estimation precision and is referred to as the Cramér-Rao bound.

The Fisher information matrix \mathcal{I} of photodetection about a set of molecule positions $\{\mathbf{R}\}$ is calculated by

$$\left[\mathcal{I}(\{\mathbf{R}\}) \right]_{(m,i);(n,j)} = \int \int P[\mathbf{r}|\{\mathbf{R}\}] \frac{\partial \ln P[\mathbf{r}|\{\mathbf{R}\}]}{\partial R_{m,i}} \frac{\partial \ln P[\mathbf{r}|\{\mathbf{R}\}]}{\partial R_{n,j}} d\mathbf{r}, \quad (\text{B2})$$

where $m, n = 1, 2, \dots, N$ and $i, j = 1, 2$. We denote $R_{m,1} = X_m$, $R_{m,2} = Y_m$ and use $(m, i); (n, j)$ as the label of the matrix element of the Fisher information matrix. We note that, in general, both the diagonal and off-diagonal elements have nonzero values. The theoretical limit on the localization precision is then given by calculating the inverse matrix of the Fisher information matrix:

$$\text{Var}[\hat{R}_{m,i}] \geq \frac{\left[\mathcal{I}^{-1}(\{\mathbf{R}\}) \right]_{(m,i);(m,i)}}{N_{\text{photon}}}. \quad (\text{B3})$$

Appendix C: Self-consistent equations and maximum likelihood estimators

In our formulation, the problem of identifying the most probable set of molecule positions is equivalent to maximizing the conditional probability distribution in Eq. (A3) with respect to possible multiple-molecule configurations $\{\mathbf{R}_{\text{est}}\} \equiv \{\mathbf{R}_1, \mathbf{R}_2, \dots, \mathbf{R}_{N_{\text{est}}}\}$. To achieve this goal, we first fix the number of molecules, N_{est} , and restrict configurations within the N_{est} -molecule configurational space. We then repeat the same procedure for other N_{est} and determine the most probable configuration based on the information-theoretic consideration as detailed below.

The estimators are given by solving the following set of N_{est} self-consistent equations:

$$\frac{\partial P[\{\mathbf{R}\}_{\text{est}} | \mathbf{r}_1, \mathbf{r}_2, \dots, \mathbf{r}_{N_{\text{photon}}}]}{\partial \mathbf{R}_m} = 0. \quad (\text{C1})$$

Since we assume no prior knowledge about the configuration of molecules, the initial distribution P_0 is chosen to be a uniform distribution. From Eqs. (A1), (A2), and (A3), we can, from analytical calculations, simplify the set of equations satisfied by the estimators as follows:

$$\mathbf{R}_m = \frac{\sum_{i=1}^{N_{\text{photon}}} \mathbf{r}_i g_m(\mathbf{r}_i; \{\mathbf{R}\}_{\text{est}})}{\sum_{i=1}^{N_{\text{photon}}} g_m(\mathbf{r}_i; \{\mathbf{R}\}_{\text{est}})}, \quad (\text{C2})$$

where $m = 1, 2, \dots, N_{\text{est}}$ denotes the label of each estimator. We then introduce the weight-function g_m by

$$g_m(\mathbf{r}; \{\mathbf{R}\}_{\text{est}}) \equiv \frac{\exp\left(-\frac{|\mathbf{r}-\mathbf{R}_m|^2}{2\sigma^2}\right)}{\gamma + \sum_{k=1}^{N_{\text{est}}} \exp\left(-\frac{|\mathbf{r}-\mathbf{R}_k|^2}{2\sigma^2}\right)}. \quad (\text{C3})$$

Here we define the term $\gamma \equiv 2\pi\sigma^2 N_{\text{est}} \epsilon / (S(1 - \epsilon))$ which describes the contribution from background noise. We note that the estimators are shown to coincide with the maximum likelihood estimator and hence, the equality in Eq. (B3) can be asymptotically attained by finding the solution of the self-consistent equations (C2). Although the conditional probability distribution may have a local maximum, the correct solution corresponding to the global maximum can be successfully obtained by the robust iterative calculation and the well-established rejection algorithm (see Appendices).

We can easily generalize the above discussions to pixelated measurements in which the number of photodetections $N_{i,j}$ at each pixel $\langle i, j \rangle$ constitutes the sufficient statistic. The result is the following set of N_{est} self-consistent equations for estimators:

$$\mathbf{R}_m = \frac{\sum_{\langle i,j \rangle} \mathbf{r}_{i,j} g_{ij;m}(\{\mathbf{R}\}_{\text{est}})}{\sum_{\langle i,j \rangle} g_{ij;m}(\{\mathbf{R}\}_{\text{est}})}, \quad (\text{C4})$$

where $\mathbf{r}_{i,j}$ is the pixel position and $g_{ij;m} \equiv N_{ij} g_m(\mathbf{r}_{i,j}; \{\mathbf{R}\}_{\text{est}})$.

Appendix D: Extension to 3D Imaging

We can also extend our method to three-dimensional imaging by the simultaneous localization of the third direction. By using a cylindrical lens into the beam path, we can

introduce the astigmatism that enables an extraction of the three-dimensional positional information as demonstrated in Ref. 27. The astigmatism introduces an asymmetric point spread function for each molecule, which is described by

$$P[\mathbf{r}|\mathbf{R}, Z] = \frac{1}{2\pi\sigma_X(Z)\sigma_Y(Z)} \exp\left(-\frac{(x-X)^2}{2\sigma_X^2(Z)} - \frac{(y-Y)^2}{2\sigma_Y^2(Z)}\right), \quad (\text{D1})$$

where the Z -dependent standard deviations of the transverse directions are defined by

$$\sigma_X(Z) = \sigma_0 \sqrt{1 + \frac{(Z-\eta)^2}{d^2}}, \quad (\text{D2})$$

$$\sigma_Y(Z) = \sigma_0 \sqrt{1 + \frac{(Z+\eta)^2}{d^2}}. \quad (\text{D3})$$

Here we define the middle point of the two perpendicular focal planes as $z = 0$ and introduce an axial astigmatism η , the focus standard deviation σ_0 , and the focal depth d .

The probability distribution of photodetections generated by multiple molecules is constructed from an incoherent sum of the asymmetric point spread functions in the same manner as in the previous section. By maximizing the conditional probability distribution with also respect to the third direction Z_m in addition to the transverse directions X_m and Y_m , we can obtain the self-consistent equations for the third direction. After some calculations, we arrive at the final result

$$Z_m = \eta \cdot \frac{\sum_{i=1}^{N_{\text{photon}}} (g_{i;m}^X - g_{i;m}^Y)}{\sum_{i=1}^{N_{\text{photon}}} (g_{i;m}^X + g_{i;m}^Y)}, \quad (\text{D4})$$

where we introduce the weight function in the X and Y directions,

$$g_{i;m}^X \equiv \frac{N_{ij} \exp\left(-\frac{(x_i-X_m)^2}{2\sigma_X^2(Z_m)} - \frac{(y_i-Y_m)^2}{2\sigma_Y^2(Z_m)}\right) \left(\frac{(x_i-X_m)^2}{\sigma_X^4(Z_m)} - \frac{1}{\sigma_X^2(Z_m)}\right)}{\gamma + \sum_{k=1}^{N_{\text{est}}} \exp\left(-\frac{(x_i-X_k)^2}{2\sigma_X^2(Z_k)} - \frac{(y_i-Y_k)^2}{2\sigma_Y^2(Z_k)}\right) / \sqrt{\left(1 + \frac{(Z_k-\eta)^2}{d^2}\right) \left(1 + \frac{(Z_k+\eta)^2}{d^2}\right)}} \quad (\text{D5})$$

$$g_{i;m}^Y \equiv \frac{N_{ij} \exp\left(-\frac{(x_i-X_m)^2}{2\sigma_X^2(Z_m)} - \frac{(y_i-Y_m)^2}{2\sigma_Y^2(Z_m)}\right) \left(\frac{(y_i-Y_m)^2}{\sigma_Y^4(Z_m)} - \frac{1}{\sigma_Y^2(Z_m)}\right)}{\gamma + \sum_{k=1}^{N_{\text{est}}} \exp\left(-\frac{(x_i-X_k)^2}{2\sigma_X^2(Z_k)} - \frac{(y_i-Y_k)^2}{2\sigma_Y^2(Z_k)}\right) / \sqrt{\left(1 + \frac{(Z_k-\eta)^2}{d^2}\right) \left(1 + \frac{(Z_k+\eta)^2}{d^2}\right)}}. \quad (\text{D6})$$

We note that $\gamma \equiv 2\pi\sigma_0^2 N_{\text{est}} \epsilon / (S(1-\epsilon))$ is defined in terms of the focus deviation σ_0 .

Appendix E: Extension in the presence of nonuniform background noise and for molecules with unequal brightness

The above formulation can be also extended to the case with nonuniform background noise. Let $\epsilon(\mathbf{r})$ be the fraction of the background noise at position \mathbf{r} . By replacing the term

γ in Eq. (C3) with the following term $\gamma(\mathbf{r})$,

$$\gamma(\mathbf{r}) \equiv \frac{2\pi\sigma^2 N\epsilon(\mathbf{r})}{S(1 - \int_S \epsilon \, d\mathbf{r}/S)}, \quad (\text{E1})$$

we can use the self-consistent equations Eq. (C2) to obtain the most probable estimators for molecule positions with nonuniform background.

We next consider generalization to molecules with unequal brightness. Let I_m be the intensity of the m th molecule. Then, by following the same procedure in the previous section, we can obtain the self-consistent equations in Eq. (C2) by replacing the function g_m by

$$g_{m,w}(\mathbf{r}; \mathbf{R}_1, \mathbf{R}_2, \dots, \mathbf{R}_{N_{\text{est}}}) \equiv \frac{\exp\left(-\frac{|\mathbf{r}-\mathbf{R}_m|^2}{2\sigma^2}\right)}{\gamma + \sum_{k=1}^{N_{\text{est}}} w_k \exp\left(-\frac{|\mathbf{r}-\mathbf{R}_k|^2}{2\sigma^2}\right)}, \quad (\text{E2})$$

where we introduce the intensity weight $w_m \equiv I_m / \sum_{n=1}^{N_{\text{est}}} I_n$. These generalizations can be applied jointly to deal with realistic situations.

Appendix F: Simultaneous localization method

1. Iterative method.

To solve the self-consistent equations, we apply the high-order iterative method known as Steffensen's method [29], which allows quadratic convergence. In contrast to an ordinary iterative method, Steffensen's method does not need to calculate derivatives and, in our problem, can efficiently perform iterative calculations. To avoid an unwanted divergence and make a robust convergence, when a temporal value of estimators becomes unreasonably high, the simple successive substitution is also concomitantly used. The iteration is terminated when the calculation either converges or 100 iterations occurred.

2. Pre-estimation and initialization.

To find the global maximum of the conditional probability distribution is an essential step for the simultaneous localization. To do so, we combine the pre-estimation and the optimization based on the information measure as follows.

First, we pre-estimate and localize molecules based on the single-molecule analysis with the well-established rejection algorithm. The local maximum is identified by setting a suitable threshold. Then, the image is fitted with a single point spread function and the position of a molecule is estimated. If the result of the fitting significantly deviates from the position of the local maximum, the image is judged as constructed from multiple molecules and the estimated position is discarded. The resulting set of N_{ini} localized positions that are not rejected by the algorithm constitutes the first set of initial positions for iterations.

Second, for each assumed number of molecules N_{est} , the residual $N_{\text{est}} - N_{\text{ini}}$ initial positions are randomly generated according to the observed probability distribution of photodetections. This enables the well-estimated initialization of estimators in successive iterative calculations. A large number of different sets of initial positions are generated and iterative calculations are performed by starting from each set (typically, preparing about a thousand of different sets is sufficient to find the global solution at the high-molecule density). The iteration result that minimizes the Kullback-Leibler divergence between the observed distribution and the distribution reconstructed from the estimated positions is chosen as the most probable set of molecule positions that reproduces the observed distribution of photodetections within the sector of N_{est} -molecule configuration space.

We note that the performance of the calculation can be enhanced by increasing both the trial number of preparing the initial configurations and the number of iterations. In this way, the fidelity of finding the global maximum of the conditional probability distribution can, in principle, be improved up to near unit fidelity.

3. Optimization method.

We perform the above procedures of estimating the most probable set of molecule positions for various molecule number $N_{\text{est}} \geq N_{\text{ini}}$. For each iteration result of the N_{est} -molecule configurational space, we calculate the expected probability distribution $P_{N_{\text{est}}}$ of photodetections and compare it with the observed probability distribution P_{data} by employing the Kullback-Leibler divergence $D[P_{\text{data}}|P_{N_{\text{est}}}]$. This information-theoretic measure gives a concrete criteria to find the true molecule configuration because, in the limit of a large number of detections, the value of the measure converges to zero only if the assumed emitter number accords with the true molecule number. Hence, among those iteration results of various

emitter numbers, the final set of the most probable molecule positions is determined by minimizing the Kullback-Leibler divergence with respect to N_{est} . We denote the final estimation result as $\{\mathbf{R}^*\} \equiv \{\mathbf{R}_1^*, \mathbf{R}_2^*, \dots, \mathbf{R}_{N_{\text{est}}^*}^*\}$.

4. Reconstruction.

The final step is to reconstruct the estimated distribution of molecules. To this end, we approximate estimation uncertainty of each molecule coordinate by calculating the diagonal element of the inverse of the Fisher information matrix because the estimators asymptotically achieves the equality in Eq. (B3). The Fisher information matrix is obtained from Eq. (B2) by replacing integration by the sum over pixels in the region of interest. Consequently, we generate the reconstructed probability distribution of molecules $P_{\text{recon}}[\mathbf{R}]$ as the sum of N_{est}^* two-dimensional Gaussian distributions $\mathcal{N}(\mathbf{R}_m^*, \frac{\mathcal{I}_m^{-1}(\{\mathbf{R}^*\})}{N_{\text{photon}}})$, where $m = 1, 2, \dots, N_{\text{est}}^*$, \mathbf{R}_m^* is the localized coordinate of molecule m , and \mathcal{I}_m^{-1} denotes the m molecule coordinates sector of the inverse of the Fisher information matrix.

[29] Burden, R. L. & Faires, J. D. *Numerical Analysis, eighth-ed.* (Brooks/Cole, 2004).